 CMC, vol.25, no.2, pp.177-193, 2011

Local Buckling Prediction for Large Wind Turbine Blades

W. Liu, X. Y. Su, Y. R. An, and K. F. Huang[1]

Abstract: Local buckling is a typical failure mode of large scale composite wind turbine blades. A procedure for predicting the onset and location of local buckling of composite wind turbine blades under aerodynamic loads is proposed in this paper. This procedure is distinct from its counterparts in adopting the pressure distributions obtained from Computational Fluid Dynamics (CFD) calculations as the loads. The finite element method is employed to investigate local buckling resistance of the composite blade. To address the mismatch between the unstructured CFD grids of the blade surface and the finite shell elements used during the buckling analysis, an interpolation code is developed, allowing mapping the pressure computed by using CFD to the finite element model. With the well documented National Renewable Energy Laboratory phase VI wind turbine blade, the procedure is demonstrated to be capable of yielding satisfactory results. Comparison with results obtained by using the blade surface pressure distributions calculated using a simple method is also conducted.

Keywords: Wind turbine blade, local buckling, CFD technique, finite element method.

1 Introduction

Development of renewable energy sources has been rapid since the emergence of energy crisis in the 1970s, and since then the urge for clean energy to moderate the greenhouse effect has been driving the research in this field. Among the main candidate renewable energy sources, wind energy is the fastest-growing one partially because of its technological maturity and relative cost competitiveness. In order to harvest energy more efficiently from the wind and due to cost-effective considerations, the size of the wind turbine has increased over the decades.

The blade is one of the most important components in a wind turbine which nowadays is designed according to refined aerodynamics in order to capture as much

[1] Peking Univ, LTCS and Dept Mech & Aero Engn, Coll Engn, Beijing 100871, China. Corresponding author, Email address: huangkefu@gmail.com (K. F. Huang).

energy as possible from the wind. Modeling of the wind turbine blade has been receiving more and more research attention (Lin, Lee and Lin, 2008). Currently most wind turbine blades are fabricated with composite materials as composite materials can satisfy complex design constraints such as lower weight and proper stiffness, while providing good resistance to the static and fatigue loading. The design of composite wind turbine blades is a challenging problem due to the need for pushing the material utilization to the limit in order to obtain light and cost effective structures. As a consequence of the minimum material design strategy, the blades are becoming thin-walled, such that structural instability or local buckling would occur. It has been recognized that while the design of the wind turbine blades was dictated by fatigue considerations in the past (Shokrieh and Rafiee, 2006), nowadays the driving design parameter within the wind turbine blade industry has shifted from fatigue issues to structural instability as the blades become larger and new materials are taken into use.

There are considerable works concerning buckling of the wind turbine blades (Bir, 2001; Hermann, Mamarthupatti and Locke, 2005; Lund and Johansen, 2008; Cairns et al, 2000; Walter et al, 2001; McKittrick et al, 2001; Kong, Bang and Sugiyama, 2005; Jensen et al, 2006). Bir (2001) developed a computerized method for preliminary structural design of composite wind turbine blades. The design code developed therein used ultimate-strength and buckling-resistance criteria. Hermann, Mamarthupatti and Locke (2005) investigated the buckling and post-buckling behavior of a wind turbine blade substructure using finite element method. The analysis was correlated with data from a static test and modified lamination schedules were provided to improve the buckling behaviour of the blade structure. Lund and Johansen (2008) proposed a multi-material topology optimization approach to obtain buckling optimized multi-material designs of wind turbine blades. Walter et al (2001) experimentally determined the buckling strength of pultruded fibreglass wind turbine blade sections and the test data were compared to the results of three analytical buckling prediction methods.

However, the aforementioned works all employed some reduced forms of loads to investigate the buckling strength of the wind turbine blades, such as four-point-bending (Hermann, Mamarthupatti and Locke, 2005; Walter et al, 2001), bending moment distribution at some positions along the spanwise direction of the blades (Bir, 2001; Kong, Bang and Sugiyama, 2005; Jensen et al, 2006). These reduced forms of loads are reasonable to some extent when the global load-carrying capability and buckling strength are to be determined. Nevertheless, as the onset and the location of local buckling are concerned, these reduced forms of loads are insufficient and more detailed load conditions such as the pressure distribution on the blade surface are requested. McKittrick et al (2001) performed buckling and

postbuckling analysis of a wind turbine blade using finite element method. The blade surface pressure they adopted therein was obtained by adjusting the dynamic pressure calculated by using Bernoulli's equation. Since the flow field around the blade is considerably complex, Bernoulli's equation is not capable of reflecting the rich physics such as stall and separation, and therefore the calculated blade surface pressure was not satisfactorily accurate. More accurate pressure distribution is needed for the prediction of the onset and the location of local buckling.

There has been an increasing interest in using Computational Fluid Dynamics (CFD) techniques to predict the aerodynamic performance and the load characteristics of wind turbines (Sezer-Uzol and Long, 2006; Laursen, Enevoldsen and Hjort, 2007; Carcangiu et al, 2007; Ferrer and Munduate, 2007; Baxevanou et al, 2008; Park, Chang and Cho, 2007). Compared with some simplified methods such as Blade Element Momentum theory, CFD methods can offer more detailed loads, such as local pressure distribution on the blade surface. It has been proved that although there are still some aspects to be explored for wind turbine application, the CFD technique is capable of consistently reproducing the experimental results such as the measured aerodynamic forces along the blade span even under highly three-dimensional (3D) and extreme stall conditions (Hansen, 2006). Thus CFD can be used to calculate the blade surface pressure which can be used as the aerodynamic loads in the prediction of the onset and location of local buckling.

In this paper, a procedure for predicting the onset and location of local buckling of composite wind turbine blades using the pressure distribution obtained from CFD is proposed. The full 3D steady RANS (Reynolds-averaged Navier–Stokes equations) approach is used to simulate the flow field around a rotating blade of a horizontal axis wind turbine and the blade surface pressure is obtained. Then the finite element method is applied to investigate the onset and location of the local buckling of the composite blade . In order to address the mismatch between the unstructured grids used to discretize the surface of the blade during CFD calculations and the shell elements used during buckling analysis, a code has been developed for mapping the pressure computed by using CFD to the finite element model. The procedure is demonstrated with the NREL phase VI wind turbine blade. Comparison with results obtained by using the pressure distribution in (McKittrick et al, 2001) is also performed.

2 Basic theory

2.1 CFD calculations

The CFD calculation is based on the steady, incompressible Reynolds-averaged Navier-Stokes (RANS) equations

$$\frac{\partial u_i}{\partial x_i} = 0 \tag{1}$$

$$\frac{\partial}{\partial x_j}(u_i u_j) = -\frac{1}{\rho}\frac{\partial p}{\partial x_i} + \nu\frac{\partial^2 u_i}{\partial x_i^2} + \frac{\partial}{\partial x_j}(-\overline{u_i' u_j'}) \tag{2}$$

Where u_i and x_i are the mean velocity component and coordinate in direction i respectively; p is the pressure; ρ is the density; ν is the dynamic viscosity of the fluid.

The Boussinesq hypothesis relates the Reynolds stresses to the mean velocity gradients

$$-\rho\overline{u_i' u_j'} = \mu_t\left(\frac{\partial u_i}{\partial x_j} + \frac{\partial u_j}{\partial x_i}\right) - \frac{2}{3}\left(\rho\kappa + \mu_t\frac{\partial u_i}{\partial x_i}\right)\delta_{ij} \tag{3}$$

Where μ_t is the turbulent viscosity, and κ is the turbulent kinetic energy.

The Spalart-Allmaras (S-A) (Spalart and Allmaras, 1994) turbulence model has been chosen to close the equations. The Spalart-Allmaras model is a one-equation model which is designed specifically for aerospace applications. It has also shown fairly good capabilities for turbomachinery applications. Since the blade is performing a steadily rotating motion, the governing equations need to be solved in the rotating frame of reference.

2.2 Linear-elastic buckling finite element analysis

The linear-elastic buckling finite element analysis of structures can be formulated as an eigenvalue problem as following (Zienkiewicz, 1989):

$$(\mathbf{K}_e + \lambda\mathbf{K}_G)\,\mathbf{U} = \mathbf{0} \tag{4}$$

Where $\mathbf{K}_e$ is the linear-elastic stiffness matrix, $\mathbf{K}_G$ the geometric stiffness matrix, λ the buckling load factor, $\mathbf{U}$ the buckling mode, respectively.

3 CFD calculation results and validation

3.1 Numerical model

The CFD computations are performed using the commercial finite-volume solver Fluent with a steady-RANS approach. The well documented two-bladed NREL

phase VI wind turbine is chosen to be simulated, mainly because there is plenty of experimental data about the aerodynamics of this turbine so that the simulation results can be benchmarked. The blade is ∼5m long, tapered and twisted along the spanwise direction. The detailed data about the geometry, the blade chord and twist distributions can be found in (Hand et al, 2001), and the configuration of the blade is shown in Fig. 1.

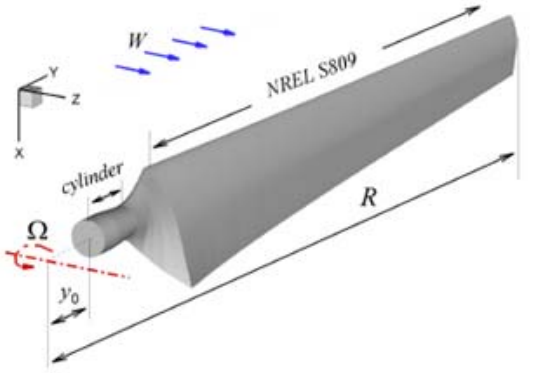

Figure 1: NREL phase VI wind turbine blade

For this study, unstructured grids have been created using tetrahedral and prismatic elements. Only one blade is modeled and periodic boundary conditions are used. In all cases fully turbulence flow is assumed. The S-A turbulence one equation model in conjunction with wall function is selected for these computations. For boundary conditions, in the upwind free stream velocities condition is given, and the range of free stream velocities is from 7m/s to 25m/s; in the downwind is the pressure outlet condition. Second order discretization schemes are used for all variables and the PRESTO algorithm is selected to solve the pressure-velocity coupling.

3.2 Numerical results and experimental validation

The outlined methodology has been applied to predict the pressure coefficient (Cp) distribution using the NREL NASA-AMES experiments (Hand et al, 2001) for validation. The simulated conditions corresponded to free stream velocities ranging from 7m/s to 25m/s and a rotational speed of 71.63rpm. Fig. 2 shows the Cp comparison between CFD and experimental data for the 30%, 47%, 63% and 80% spanwise stations with a free stream velocity of 15m/s. It can be seen that the CFD computations are able to reproduce quite accurately the experimental Cp values at these locations, except that there are some discrepancies at the 30% spanwise sta-

tion, which are thought to be due to the effect of the tower that is temporarily not considered in the simulations.

One can naturally figure out that the results such as the pressure distributions obtained by CFD can be used in the structural design of the wind turbine blade. However when finite element shell model of the blade is employed in the structural design, which is often the case especially as the blade is becoming larger and larger, the number of the shell elements is generally much less than that of the unstructured grids that are used to discretize the surface of the blade and on which the blade surface pressures are obtained during the CFD calculations. This mismatch will be addressed and the surface pressures obtained from CFD will be mapped to the finite element model of the blade to perform buckling analysis in the following sections.

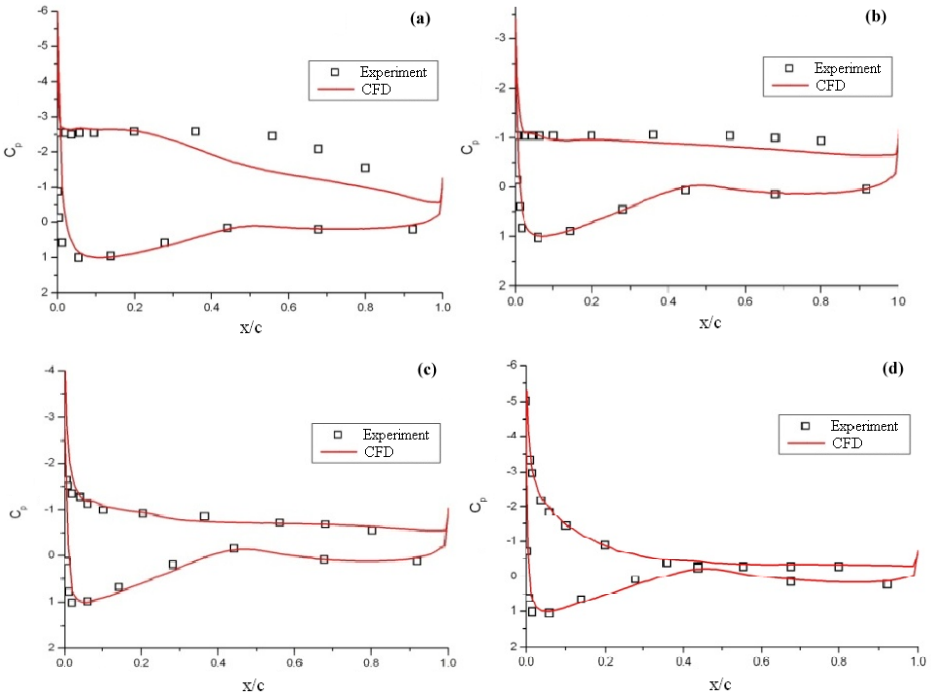

Figure 2: Pressure coefficient distributions at (a) 30% spanwise station, (b) 47% spanwise station, (c) 63% spanwise station, and (d) 80% spanwise station, with a free stream velocity of 15m/s.

4 Buckling analysis of the blade

The wind turbine blade is usually modeled as 3D beams owing to small scale and high aspect ratio in the past. However, as the scale of the blade becomes larger and larger and composite materials are taken into use, the blade is actually a class of thin-walled shell structure. In order to capture the mechanical behavior of the blade more accurately, detailed finite element models such as 3D shell models are being frequently used in the investigation and design of the wind turbine blade. In this paper, 3D finite element shell model is employed to predict the onset and location of local buckling of the wind turbine blade.

4.1 Blade geometry and components

In order to make use of the aerodynamic loads calculated using CFD in *section 3*, again the NREL phase VI wind turbine blade is chosen to be modeled and to perform the buckling analysis.

The root of the blade starts at the hub connection, at a radius 0.508m from the centre of the hub. The blade has a cylinder with 0.218m diameter extending from 0.508m to 0.660m and then tapers to a diameter 0.183 from 0.660m to 0.883m along the spanwise direction. There is a transition from the circular section at the 0.883m spanwise station to a 0.737m chord S809 airfoil at the 1.257m. Outboard from 1.257m to the tip, the blade, having the S809 airfoil, is linearly tapered and nonlinearly twisted along the spanwise direction. The detailed data pertinent to the geometry of the investigated blade is listed in (Hand et al, 2001) and the geometric model of the blade built with the finite element package ANSYS is shown in Fig. 3(a).

The investigated blade consists of two primary components: shell and web, displayed in the cross-section shown in Fig. 3(b). The shell is responsible to help create the required pressure distribution on the blade. The leading edge of the upper and lower shell and the web of the blade compose a D-spar, which is also called the main beam and supports loads on the blade that arise from different sources.

4.2 Blade layup

Since detailed 3D finite element shell model is to be employed to investigate the onset and location of the local buckling, the layup of the composite blade is a prerequisite for this investigation. Although we tried our best we did not find any information about the original composite layup of the NREL phase VI wind turbine blade in open literature. However, fortunately the purpose of this paper is to propose and demonstrate a procedure for local buckling prediction for wind turbine blades, we need not focus on a specific layup. Hereby, referring to (McKittrick et

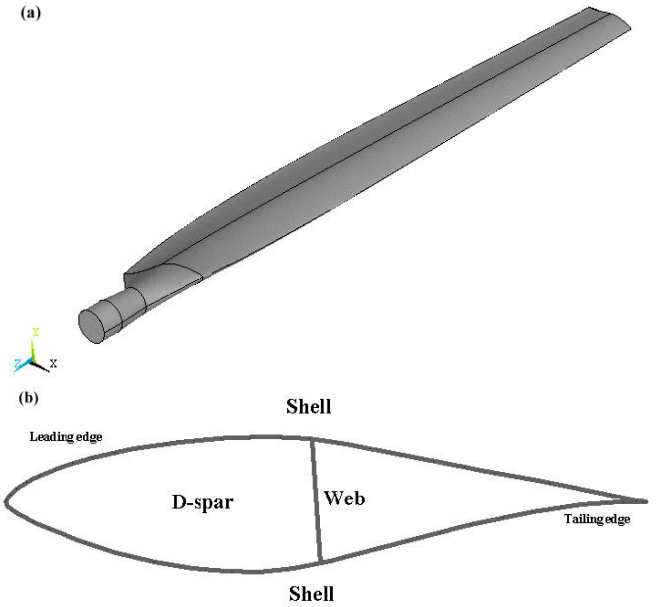

Figure 3: (a) The geometrical model, and (b) the cross-section, of the NREL phase VI wind turbine blade.

al, 2001), a generic composite layup is designed in this paper for the NREL phase VI wind turbine blade and for the local buckling investigation purpose.

According to the designed composite layup of the blade, the cylindrical sections, the transition section and the D-spar (the main beam) are relatively stiffer than the tailing edge of the shell structure as the former supports most of the loads. The detailed layup schedule of the blade is presented in Tab. 1.

Each of the GRP layers in the layup is modeled as orthotropic in a given layer, with two of the principal material axes in the plane of the shell. The orientation of the material axes (fibre directions) varies from one layer to the next. Material parameters listed in Tab. 2 are used to model various layers in the GRP layup.

Table 1: The layup schedule of the composite wind turbine blade

Component	Layup schedule
Cylindrical sections & D spar	$[\pm 45/0_3/\pm 45/0_3/+45]_s$
Tailing edge of the shell structure	[±45/0/Balsa/0/±45]

The parameters listed in Tab. 2 are derived from experimental data (Mandell and

Table 2: Material mechanical properties

Material property	A130(0°)	DB120(±45°)	Balsa wood
E_x (GPa)	31.7	26.2	0.187
E_y (GPa)	7.58	6.55	0.061
E_z (GPa)	7.58	6.55	4.07
υ_{xy}	0.32	0.39	0.67
υ_{yz}	0.32	0.35	0.01
υ_{xz}	0.32	0.32	0.02
G_{xy} (GPa)	3.45	4.14	0.020
G_{yz} (GPa)	3.10	3.72	0.150
G_{xz} (GPa)	3.10	3.72	0.220
ρ (kg/m^3)	1714	1714	153
thickness (mm)	0.571	0.203	9.53

Samborsky, 1997). The Al30 and DB120 lamina use E-glass fibres that are embedded in polymer matrix. The A130 lamina is considered for the 0 degree ply layups, while the DB120 lamina is used for the ±45 degree ply layups. The balsa wood is used as the filler in sandwich-type layups to increase the buckling resistance while minimizing the weight.

4.3 Finite element model

The structure of the composite blade is modeled with layered shell elements (element type SHELL99) capable of representing layer characteristics throughout the shell thickness. Shell99, which is designed to model thin composite plates and shell structures, has eight nodes with six degrees of freedom at each node: translations in the nodal X, Y, and Z directions and rotations about the nodal X-, Y -, and Z-axes.

Meshing size is well chosen to obtain reliable results. The number of the elements and that of the nodes are 21295 and 63416, respectively. Fig. 4 shows the finite element discretization of the blade. At the root end of the blade, the connection to the hub is assumed to be rigid, relative to the blade. As a consequence, all six degrees of freedom for the nodes in the root plane of the blade (0.508m from the hub centre) are fixed.

4.4 Loads

In *section 3*, the surface pressure distributions of the NREL phase VI wind turbine blade under six different wind speeds ranged from 7m/s to 25m/s have been calculated using CFD technique. As an example, the blade surface pressure under the

15m/s wind speed is shown in Fig. 5.

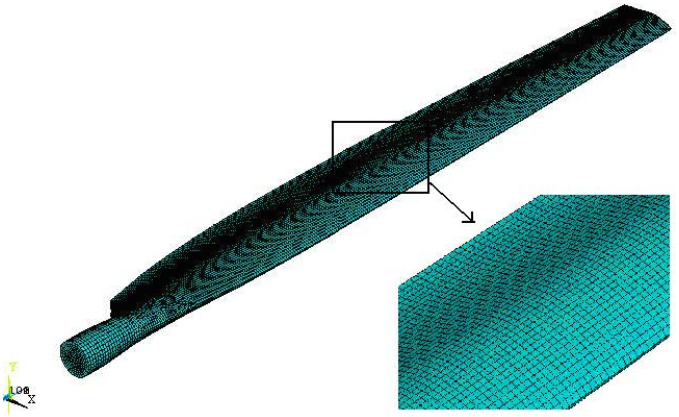

Figure 4: The finite element mesh of the NREL phase VI wind turbine blade

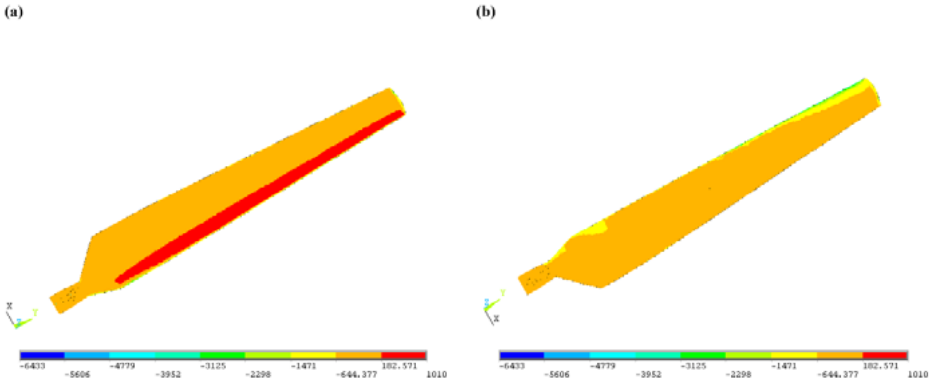

Figure 5: The pressure distribution obtained from CFD calculation (wind speed: 15m/s), (a) upper surface; (b) lower surface.

It should be noted that the number of unstructured grids used to discretize the surface of the blade during CFD calculations is 242786, which is much greater than that of the shell elements of the finite element model of the blade, 21295. To address this mismatch, an interpolation code using a search algorithm is developed, allowing the pressures on the CFD grids mapped to the finite shell elements of the blade.

Using the aforementioned code, the blade surface pressures under six wind speeds calculated using CFD technique in *section 3* are all mapped to the finite element model of the blade. Fig. 6 shows the pressure applied to the finite element model of the blade, corresponding to the 15m/s wind speed. It can be recognized that this data transfer process from the CFD model to the FEM model is effective and of considerable accuracy, which is of importance for the following local buckling analysis of the blade.

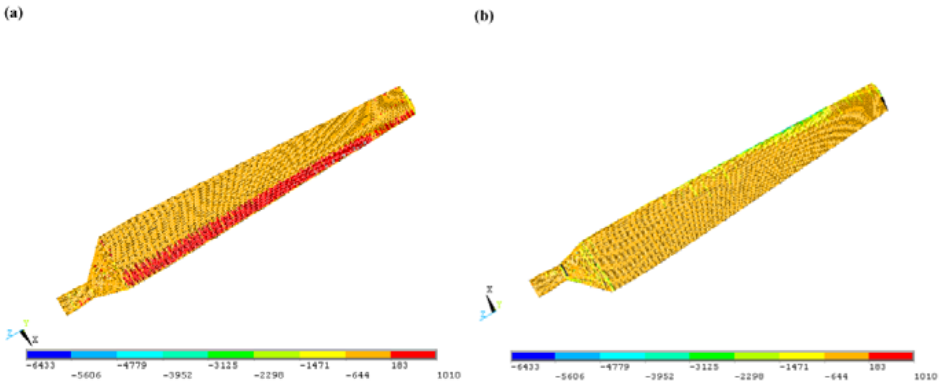

Figure 6: The pressure distribution applied to the FE model of the blade (wind speed: 15m/s), (a) upper surface; (b) lower surface.

4.5 Numerical results and discussions

With the surface pressures calculated using CFD as the loads, the buckling analysis of the composite wind turbine blade are performed in this section. The effect of the centrifugal force is taken into account by setting the blade rotating at the rated rotational speed of 71.63 rpm. The buckling analysis under six wind speeds has been performed.

The buckling load factors (magnification factors of the real loads, showing whether the structure being investigated is safe (>1) or not (<1).) and buckling shapes of the first 4 buckling modes of the blade under each of the six wind speeds considered are obtained through the buckling analysis performed previously. The load factors are listed in Tab. 3 and the buckling shapes of the first 4 buckling modes under the 15m/s wind speed are shown in Fig. 7.

It can be seen from Fig. 7 that local buckling located at the maximum chord section of the blade rather than global buckling will firstly occur if the loads (wind-induced

Table 3: Load factors of the first 4 buckling modes under the six wind speeds

Wind speed	1st	2nd	3rd	4th
7 m/s	63.450	68.033	80.695	83.273
10 m/s	30.868	33.453	40.353	41.910
13 m/s	28.912	31.330	38.022	39.534
15 m/s	29.711	32.139	39.230	40.747
20 m/s	22.813	24.593	30.086	31.208
25 m/s	16.375	17.683	21.684	22.520

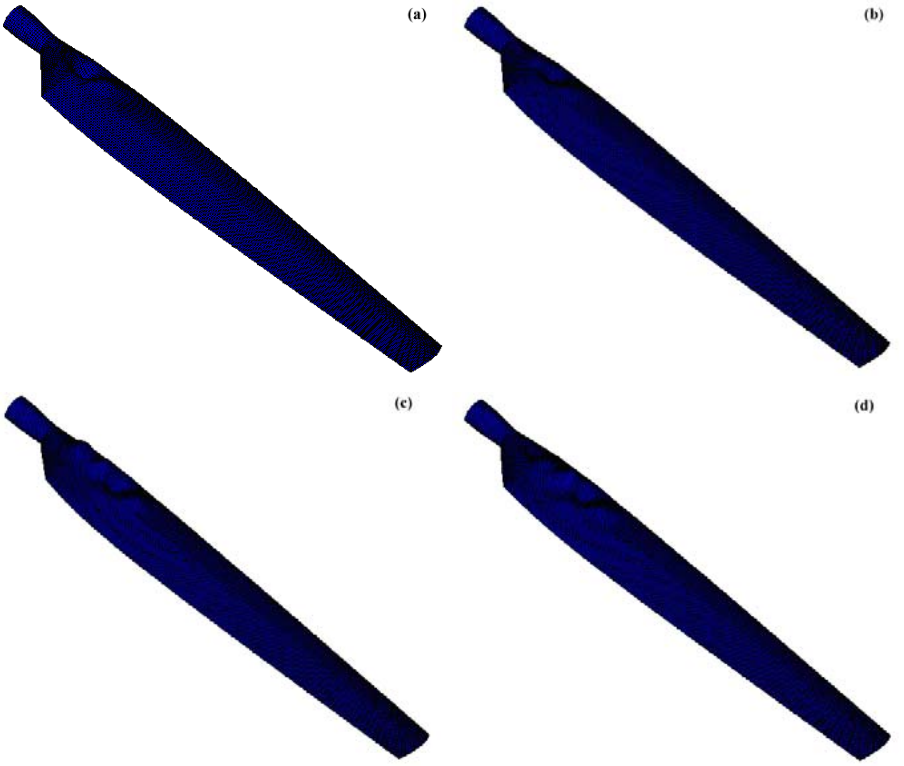

Figure 7: Buckling shapes of the (a) 1st, (b) 2nd, (c) 3rd, and (d) 4th buckling modes. Wind speed: 15m/s

pressures) increase gradually. The load factors listed in Tab. 3 are all far bigger than unity, indicating that the blade is safe under those wind speeds.

In order to obtain some intuitive knowledge about the complex relation between

buckling load factor and wind speed, load factors of the first buckling modes (which are often practically concerned) versus the corresponding wind speeds are plotted in Fig. 8.

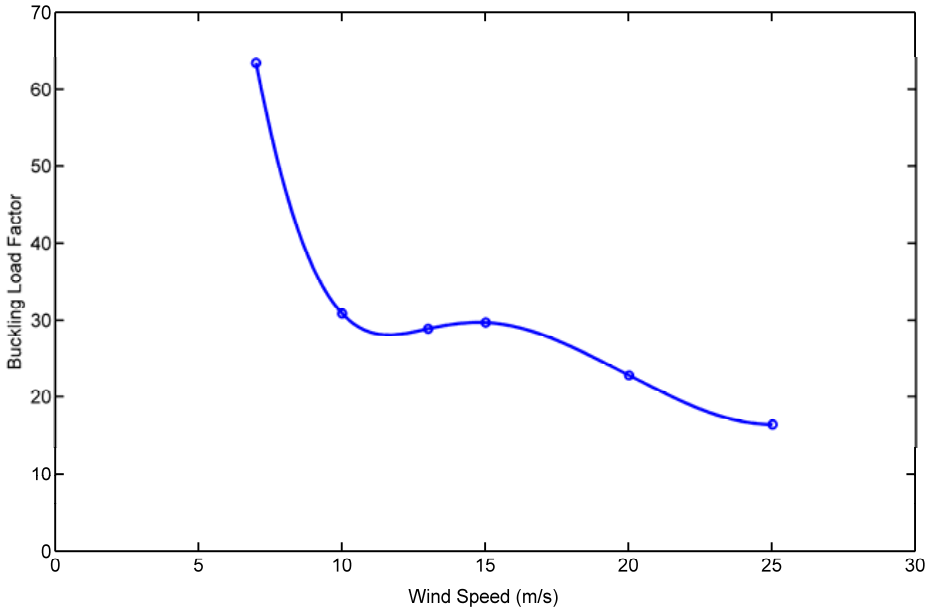

Figure 8: Load factors for different wind speeds

The relationship between buckling load factor and wind speed displays some kind of nonlinearity. Load factor decreases rapidly when wind speed increases from 7m/s to ∼11m/s; and after that load factor decreases smoothly with wind speed increasing to 25m/s. It is somewhat interesting to see that load factor for the 15m/s wind speed is a little greater than that for the 13m/s wind speed, which is explained here as the result of the deep stall phenomena induced blade surface pressures slight decrease. Because of the same mechanism, a similar phenomenon can be observed in the torque-wind speed relation curve obtained from CFD calculations and wind tunnel tests presented in (Hand et al, 2001). It is indicated that CFD techniques can effectively predict the load characteristics of wind turbines and it is reasonable to adopt pressure distributions obtained from CFD calculations to perform the buckling analysis or other structural analysis of wind turbine blades.

For the sake of comparison, buckling analysis with the blade surface pressure distributions calculated using the method adopted by McKittrick et al (2001) have also been conducted. The load factors obtained are listed in Tab. 4 and depicted

in Fig. 9 versus the wind speed, compared with the results obtained from previous buckling analysis with CFD loads.

Table 4: Load factors of the first buckling modes from the blade surface pressure distributions calculated using the method adopted by McKittrick et al (2001).

Wind speed(m/s)	7	10	13	15	20	25
Load factor	938.36	671.02	183.73	82.017	29.426	16.09

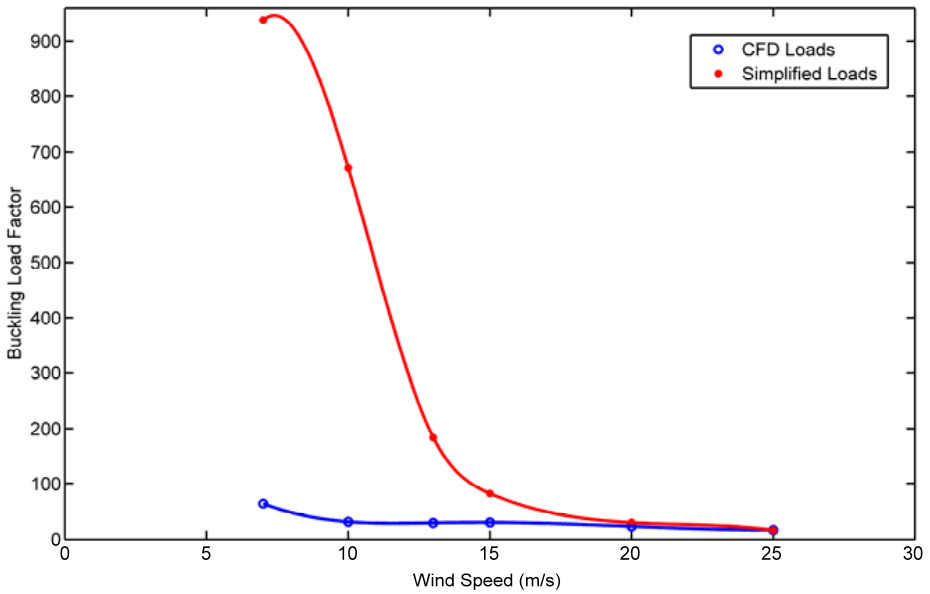

Figure 9: Comparison of Load factors resulted from using CFD loads and reduced pressure distributions

It is indicated in Tab. 4 and Fig. 9 that load factors calculated using the blade surface pressure distributions calculated using the method in (McKittrick et al, 2001) are incredibly great for low wind speeds (7, 10m/s) and sharply decrease with wind speed increases, approaching the results obtained using CFD loads when wind speed approaches 25m/s. It's obvious that this kind of simple method cannot obtain accurate blade surface pressure distributions, and therefore cannot yield satisfactory results when the loads from this method are used in structural analysis of the wind turbine blade.

5 Concluding remarks

In this paper, a procedure for predicting the onset and location of local buckling of composite wind turbine blades is developed. In this procedure, CFD techniques are first used to simulate the flow field around a rotating blade of a horizontal axis wind turbine and to obtain the blade surface pressures. Then the finite element method is employed to investigate the onset and location of the local buckling of the composite blade. Between these two steps, an interpolation code is developed to address the mismatch between the unstructured CFD grids of the blade surface and the finite shell elements used during buckling analysis, allowing mapping the pressure computed by using CFD to the finite element model. The procedure is demonstrated with a well documented wind turbine blade and comparison with results obtained by using the pressure distributions in (McKittrick et al, 2001) is also performed. The primary conclusions of this study can be drawn as follows:

The load factors obtained from the buckling analysis are all far bigger than unity, indicating that the blade is safe under the wind speeds considered here. Local buckling located at the maximum chord section of the blade is more likely to occur than global buckling. Attention should be paid to the thickness of the shell relative to the length of the blade during the blade design or setting some webs at proper positions.

The buckling load factor and the wind speed have some kind of nonlinear relation. In detail, the load factor decreases rapidly when the wind speed increases from 7m/s to $\sim$11m/s; and after that the load factor decreases smoothly with the wind speed increasing. Here load factor for 15m/s wind speed is a little greater than that for the 13m/s wind speed, which is explained here as the result of deeply stall induced blade surface pressures slight decrease.

CFD techniques can effectively predict the load characteristics of wind turbines and it is reasonable to employ pressure distributions obtained from CFD calculations as load conditions to perform buckling analysis or other structural analysis of wind turbine blade. The blade surface pressure distributions obtained from some simple methods such as the method adopted in (McKittrick et al, 2001) are usually not accurate, and therefore cannot yield satisfactory results when the loads from this class of methods are used in structural analysis of the wind turbine blade.

Acknowledgement: The study presented here is conducted in support of project supported by the State Key Development Program for Basic Research of China (Grant No. 2007CB714603). The authors acknowledge all the participants of the project and their contributions.

References

Baxevanou, C.A.; Chaviaropoulos, P.K.; Voutsinas, S.G.; Vlachos, N.S. (2008): Evaluation study of a Navier-Stokes CFD aeroelastic model of wind turbine airfoils in classical flutter. *Journal of Wind Engineering and Industrial Aerodynamics*, vol. 96, pp. 1425-1443.

Bir, G. S. (2001): Computerized method for preliminary structural design of composite wind turbine blades. *Journal of Solar Energy Engineering-Transactions of the Asme*, vol. 123, no. 4, pp. 372-381.

Cairns, D. S.; Mandell, J. F.; Sears, A.; McKittrick, L. R. (2000): Design considerations for buckling in composite wind turbine blades. *ASME Wind Energy Symposium, AIAA-2000-0059, ASME/AIAA,* pp. 354-366.

Carcangiu, C.E.; Sorensen, J.N.; Cambuli, F.; Mandas, N. (2007): CFD-RANS analysis of the rotational effects on the boundary layer of wind turbine blades. *Journal of Physics: Conference Series*, vol. 75, 012031.

Ferrer, E.; Munduate, X. (2007): Wind turbine blade tip comparison using CFD. *Journal of Physics: Conference Series*, vol. 75, 012005

Hand, M. M.; Simms, D. A.; Fingersh, L. J.; Jager, D. W.; Cotrell, J. R.; Schreck, S. J.; Larwood, S. M. (2001): Unsteady aerodynamics experiment phase VI: wind tunnel test configurations and available data campaigns. *Tech. Rep. NREL/TP-500-29955, NREL.*

Hansen, M.O.L.; Sorensen, J.N.; Voutsinas, S.; Sorensen, N.; Madsen, H.A. (2006) State of the art in wind turbine aerodynamics and aeroelasticity. *Progress in Aerospace Sciences*, vol.42, no.4, pp. 285-330.

Hermann, T.M.; Mamarthupatti, D.; Locke, J.E. (2005): Postbuckling analysis of a wind turbine blade substructure. *Journal of Solar Energy Engineering-Transactions of the Asme*, vol. 127, no. 4, pp. 544-552.

Jensen, F.M.; Falzon, B.G.; Ankersen, J.; Stang, H. (2006): Structural testing and numerical simulation of a 34 m composite wind turbine blade. *Composite Structures*, vol. 76**,** pp. 52-61.

Kong, C.; Bang, J.; Sugiyama, Y. (2005) Structural investigation of composite wind turbine blade considering various load cases and fatigue life. *Energy*, vol. 30, pp. 2101-2114.

Laursen, J.; Enevoldsen, P.; Hjort, S. (2007): 3D CFD quantification of the performance of a multi-megawatt wind turbine. *Journal of Physics: Conference Series*, vol. 75, 012007.

Lin, S. M.; Lee, S. Y.; Lin, Y. S. (2008): Modeling and bending vibration of the blade of a horizontal-axis wind power turbine. *CMES: Computer Modeling in*

Engineering & Sciences, vol. 23, no. 3, pp. 175-186.

Lund, E.; Johansen, L.S. (2008): On Buckling Optimization of a Wind Turbine Blade. *Mechanical Response of Composites*, vol. 10, pp. 243-260.

Mandell, J. F.; Samborsky, D. D. (1997): DOE/MSU composite material fatigue database: Test methods, materials, and analysis. *Contractor Report SAND97-3002, Sandia National Laboratories, Albuquerque, NM, USA*.

McKittrick, L. R.; Cairns, D. S.; Mandell, J.; Combs, D. C.; Rabern, D. A.; Van Luchene, R. D. (2001): Analysis of a Composite Blade Design for the AOC 15/50 Wind Turbine Using a Finite Element Method. *Tech. Rep. SAND2001-1441, Sandia National Laboratories*.

Park, Y.; Chang, B.; Cho, T. (2007): Numerical simulation of wind turbine scale effects by using CFD. *AIAA paper*, no. 2007-2216.

Sezer-Uzol, N; Long, L. N. (2006): 3-D time-accurate CFD simulations of wind turbine rotor flow fields. *AIAA paper*, no. 2006-0394.

Shokrieh, M.M.; Rafiee, R. (2006): Simulation of fatigue failure in a full composite wind turbine blade. *Composite Structures*, vol. 74, no. 3, pp. 332-342.

Spalart, P.R.; Allmaras, S.R. (1994): A one-equation turbulence model for aerodynamic flows. *La Recherche Aerospatiale*, no. 1, pp. 5–21.

Walter, D; Musial, B. B.; Scott D. H.; **Zutec, M. D.** (2001): Four-Point Bending Strength Testing of Pultruded Fiberglass Wind Turbine Blade Sections, *AWEA's WINDPOWER 2001 Conference,* Washington, D.C..

Zienkiewicz, O.C. (1989): *The Finite Element Method*. McGraw-Hill.